Fitting equations for the sorption isotherms of cement mortar with salt spray deposition

Frontiers of Architectural Research 15 (2026) 845–857

Available online at www.sciencedirect.com

ScienceDirect

journal homepage: www.keaipublishing.com/foar

RESEARCH ARTICLE

Fitting equations for the sorption isotherms of cement mortar with salt spray deposition

Bing Li [a,b,*], Roberto Giordano [b], Jean-Marc Tulliani [c], Saierjiang Halike [a,**], Wanjiang Wang [a], Qinglin Meng [d]

[a] School of Civil Engineering and Architecture, Xinjiang University, Urumqi 830047, China
[b] Department of Architecture and Design, Politecnico di Torino, Torino 10125, Italy
[c] Department of Applied Science and Technology, Politecnico di Torino, Torino 10129, Italy
[d] State Key Laboratory of Subtropical Building and Urban Science, South China University of Technology, Guangzhou 510641, China

Received 6 May 2025; received in revised form 2 July 2025; accepted 7 August 2025

KEYWORDS
Salt spray climate;
Cement mortar;
Sorption isotherm;
Fitting equations

Abstract The sorption isotherm of porous building materials serves as a critical hygrothermal property that regulates coupled heat and moisture transfer and influences the energy efficiency of building envelopes. Coastal buildings endure chronic salt spray exposure, yet classical fitting equations neglect salt deposition effects. This study investigates cement mortar specimens subjected to accelerated salt spray tests (0–35 cycles). The salt content of the specimens was quantified via chloride ion analysis, and isothermal sorption tests were conducted under 33%–93% relative humidity (RH) using a static equilibrium method. A modified model integrating a salt influence factor (η_u) into classical equations was developed. Additionally, dual-regime sorption isotherm models were formulated based on deliquescence mechanisms of salt crystals above critical humidity, governed by the Robinson equation and Nielsen model, respectively. This framework enables accurate prediction of equilibrium moisture content under varying coupled humidity-salt conditions, significantly enhancing the reliability of hygrothermal simulations for coastal buildings in salt spray climates.

* Corresponding author. School of Civil Engineering and Architecture, Xinjiang University, Urumqi 830047, China.
** Corresponding author.
E-mail addresses: libing@xju.edu.cn (B. Li), saierjiang@xju.edu.cn (S. Halike).
Peer review under the responsibility of Southeast University.

https://doi.org/10.1016/j.foar.2025.08.005

1. Introduction

The sorption isotherm of porous building materials quantifies equilibrium moisture content (EMC) under varying environmental humidity, serving as a critical indicator of their intrinsic hygroscopicity and dynamic moisture storage behavior (Brambilla and Sangiorgio, 2021a; Taher and Brouwers, 2023). EMC directly influences key thermophysical properties—such as specific heat capacity (C_p), thermal conductivity (λ), and water vapor permeability (δ_p)—which govern coupled heat and moisture transfer processes in building envelopes (Hung Anh and Pásztory, 2021; Kočí et al., 2016; Kontoleon and Giarma, 2016). These processes, in turn, significantly impact indoor thermal comfort, HVAC energy consumption, and operational carbon emissions (Brambilla and Sangiorgio, 2021b; Khoukhi, 2018; Liu et al., 2017). Consequently, precise quantification of EMC is fundamental for achieving reliable hygrothermal simulations and enabling energy-optimized building design.

However, in coastal salt spray climates, salt crystallization deposition modifies the sorption isotherms of building materials through deliquescence/crystallization phase transitions and pore structure evolution (Castellazzi et al., 2016; Espinosa et al., 2008; Prat, 2024; Taher and Brouwers, 2023). Classical sorption models (e.g., BET (Brunauer et al., 1938), Oswin (1946), Caurie (1970), Henderson (1973), Peleg (1993) and GAB (Berg and Bruin, 1981))—while highly accurate for salt-free materials—neglect salt—humidity coupling, limiting their applicability to building materials in coastal environments. Although Feng (Feng et al., 2013; Feng, 2014) proposed empirical equations for materials with varying hygroscopicity, these remain invalid for salt-contaminated systems. Recent studies by Bai et al. (2021) and He et al. (2023) investigated the sorption isotherms of salt-contaminated cement mortar and aerated concrete but adopted full-immersion salt infiltration, failing to replicate the natural cyclic deposition patterns of salt spray. Under natural exposure, airborne salts are transported by wind and deposited on building envelopes, subsequently migrating inward via capillary water transport. Evaporation of the absorbed moisture concentrates the salt solution within pores, ultimately triggering salt crystallization when pore solutions reach supersaturation (Morillas et al., 2020; Su et al., 2022). Salt impacts hygroscopicity through two synergistic mechanisms:

(1) Crystallization-driven microstructural changes: Salt crystallization induces pore structure alterations—such as porosity, pore size distribution, and connectivity changes—which critically modify the capillary sorption kinetics and hydraulic permeability of porous building materials (Koniorczyk and Gawin, 2008; Todorović and Janssen, 2018), as rigorously validated by our prior studies on cement mortar (Li et al., 2023, 2024a, 2024b).
(2) Deliquescence-induced moisture uptake: Hygroscopic salts (e.g., NaCl) absorb moisture at sub-saturation RH levels via water activity equilibration between pore solutions and ambient vapor, amplifying moisture retention proportionally to salt content (Lubelli et al., 2004; Méndez-Bermúdez et al., 2016). This thermodynamic process is quantified by the Robinson—Stokes equation (Horvath, 1985) and Nielsen model (Koronthalyova et al., 2015).

Consequently, the isothermal sorption behavior of salt-contaminated materials is governed by coupled humidity-salt interactions rather than humidity solely (Franzen and Mirwald, 2009; Koniorczyk and Wojciechowski, 2009). However, despite these mechanistic insights, a unified sorption model capable of explicitly integrating simultaneous humidity and salt content variations remains absent. This critical gap compromises the predictive accuracy of hygrothermal simulations in salt-laden coastal environments, directly impeding energy efficiency optimization and durability assessments for critical infrastructure.

Building upon our prior investigations into chloride ion migration, salt crystallization patterns, and microstructural evolution in cement mortar under partial immersion and accelerated salt spray conditions (Li et al., 2023, 2024b), this study advances the understanding of moisture-salt coupling mechanisms by quantifying the evolution of hygroscopicity under cyclic salt spray exposure. Previous experiments have elucidated that pore structure alterations and capillary absorption dynamics synergistically govern salt-water transport and salt crystal distribution in cement-based materials. Here, we systematically investigate how salt deposition modulates the sorption isotherm of cement mortar across varying salt spray cycles (0—35 cycles). By developing modified dual-segment fitting functions rooted in the Robinson—Stokes equation and Nielsen model, this framework enables precise prediction of EMC in salt-laden cement mortar. The findings provide a theoretical foundation for energy efficiency enhancement of coastal buildings in salt spray climates, aligning with China's "Dual Carbon" goals through optimized hygrothermal design strategies.

2. Materials and methods

2.1. Raw materials and specimen fabrication

Cement mortar was prepared using CEM II/BLL 32.5R cement (Italy), standardized silica sand (BS EN 197-1: 2011), and deionized water. The cement, widely used in masonry structures, mainly comprises 65%—79% clinker and 21%—35% limestone. A cement-to-sand-to-water mass ratio of 1:3:0.5 was adopted. Fresh mortar was cast into $40 \times 40 \times 160$ mm^3 steel molds in three layers, compacted via mechanical vibration, and cured for 24 h at 23 ± 1 °C and 95% ± 2% RH, followed by demolding and 28-day water immersion curing at 23 ± 2 °C (Fig. 1(a)).

To expedite isothermal sorption equilibrium tests, the reduced-size specimens were commonly adopted (Jamali et al., 2006; Swami et al., 2005). Direct molding of thin cement mortar specimens proved challenging due to compromised compaction and surface uniformity. So, $40 \times 40 \times 10$ mm^3 thin specimens were sectioned from full-sized counterparts (Fig. 1(b)). Sectioned slices were cleaned with compressed air and deionized water to remove surface particles and prevent pore blockage (Fig. 1(c)). Specimens were labeled and dried at 55 ± 2 °C in a forced-convection oven—a temperature optimized to ensure complete moisture removal while preserving the native pore structure by preventing

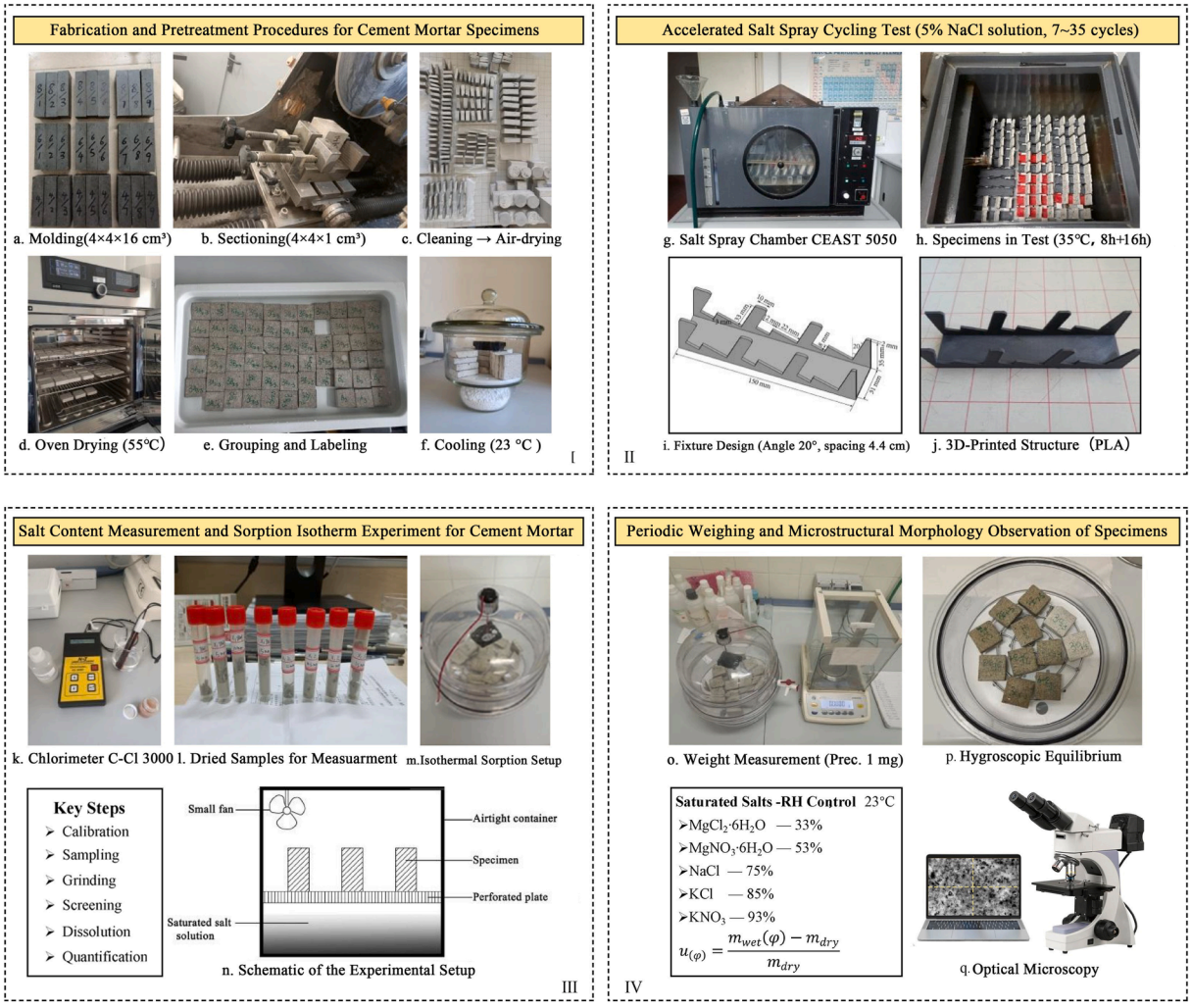

Fig. 1 Key Instruments and parameters in the experiment.

thermal degradation of critical hydration products—until achieving constant mass (<0.1% weight variation over 24 h), following ISO 12570:2000) (Fig. 1(d) (e)). The dried specimens were then cooled to room temperature (23°C) in a desiccator before testing (Fig. 1(f)). Although the cutting process may induce partial damage to the surface pore structure of the specimens, the EMC is dominated by the vast majority of internal micro-pores. This cutting methodology has also been utilized in previous investigations on aerated concrete, calcium silicate boards, and ceramic tiles (Feng, 2014; Peuhkuri et al., 2005).

2.2. Cyclic salt spray exposure

Salt deposition on building materials evolves gradually under natural climatic fluctuations. To simulate the hygroscopic behavior of porous materials in coastal salt spray environments, a cyclic spray-dry protocol was implemented. While standards such as BS EN 14147:2003 and B117—2011 primarily address natural stone durability, this study adapts their principles to cement mortar by optimizing temporal parameters. To mimic diurnal natural cycles and ensure complete moisture absorption/drying, the spray-dry duration ratio (1:2) was maintained, but the 12-h cycle (4 h spray + 8 h dry) was extended to a 24-h cycle (8 h spray + 16 h dry). The protocol specified a spray temperature of 35 °C, drying temperature of 55 °C, and a mean deposition rate of 2 mL/80 cm^2/h. A CEAST 5050 salt spray chamber (Figs. 1(g)—Fig. 2) was utilized to generate 5 wt% NaCl fog (pH 6.5—7.2). Specimens were positioned at a 20° angle from vertical with 44 mm spacing during testing (Fig. 1(h)(i)(j)).

A total of 90 specimens were allocated into six groups (0 [control], 7, 14, 21, 28, 35 cycles). Post-exposure, each group was subdivided for isothermal sorption testing at 33%, 53%, 75%, 85%, and 93% RH. Triplicate specimens per condition ensured statistical validity (Table 1).

2.3. Salt content analysis

To quantify salt deposition in cement mortar under cyclic salt spray exposure, chloride ion (Cl^-) concentration was measured as a proxy for NaCl accumulation. Specimens subjected to varying spray cycles were analyzed using a chlorimeter (C-CL-3000, James Instruments, USA), which

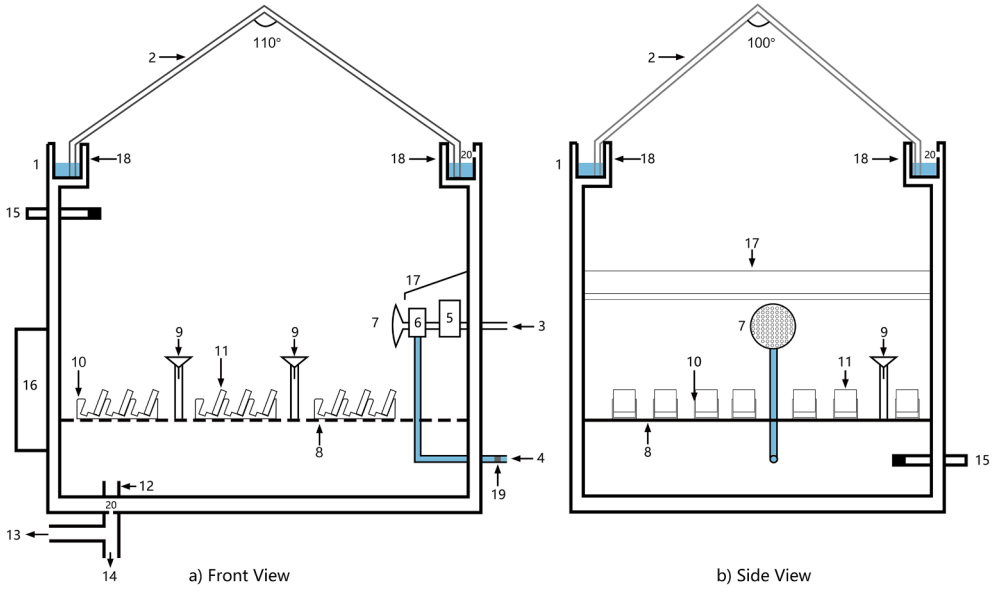

Fig. 2 Internal schematic of the CEAST 5050 salt spray chamber.

Table 1 Cement mortar specimens grouped by salt spray exposure cycles and ambient humidity conditions.

Ambient RH (%)	Reference	7 Cycles	14 Cycles	21 Cycles	28 Cycles	35 Cycles
33	3O1-1, 3O2-1, 3O3-1	3A1-1, 3A2-1, 3A3-1	3A1-2, 3A2-2, 3A3-2	3A1-3, 3A2-3, 3A3-3	3A1-4, 3A2-4, 3A3-4	3A1-5, 3A2-5, 3A3-5
53	3O1-2, 3O2-2, 3O3-2	3B1-1, 3B2-1, 3B3-1	3B1-2, 3B2-2, 3B3-2	3B1-3, 3B2-3, 3B3-3	3B1-4, 3B2-4, 3B3-4	3B1-5, 3B2-5, 3B3-5
75	3O1-3, 3O2-3, 3O3-3	3C1-1, 3C2-1, 3C3-1	3C1-2, 3C2-2, 3C3-2	3C1-3, 3C2-3, 3C3-3	3C1-4, 3C2-4, 3C3-4	3C1-5, 3C2-5, 3C3-5
85	3O1-4, 3O2-4, 3O3-4	3D1-1, 3D2-1, 3D3-1	3D1-2, 3D2-2, 3D3-2	3D1-3, 3D2-3, 3D3-3	3D1-4, 3D2-4, 3D3-4	3D1-5, 3D2-5, 3D3-5
93	3O1-5, 3O2-5, 3O3-5	3E1-1, 3E2-1, 3E3-1	3E1-2, 3E2-2, 3E3-2	3E1-3, 3E2-3, 3E3-3	3E1-4, 3E2-4, 3E3-4	3E1-5, 3E2-5, 3E3-5

Table 2 Calibration of saturated salt solutions: theoretical vs. measured (RH) at 23 °C.

NO.	Saturated salt solution	Relative Humidity (RH, %)		Relative deviation(%)
		Theoretical value	Measured value	
1	$MgCl_2 \cdot 6H_2O$	33	32.9	−0.30
2	$Mg(NO_3)_2 \cdot 6H_2O$	53	53.5	0.94
3	NaCl	75	75.2	0.27
4	KCl	85	84.9	−0.12
5	KNO_3	93	93.6	0.65

quantifies Cl^- via detecting voltage changes induced by electrochemical reactions in acidic solutions (Fig. 1(k)).

Prior to testing, the electrode was calibrated with 0.005%, 0.01%, 0.05%, 0.1%, and 0.3% Cl^- reference solutions. Full-thickness samples were ground to homogenize salt distribution, and 3 g dried aliquots were dissolved in 20 mL acid solution (Fig. 1(k) (l)). After 2-min stabilization and gas release, measurements were conducted at 23 ± 1 °C. All tests were completed within 2 h post-calibration to ensure accuracy.

2.4. Isothermal sorption testing

This study investigated the equilibrium moisture content of salt-contaminated cement mortar under varying relative humidity (33%—93% RH) and salt spray cycles (0—35 cycles) via the static desiccator method ISO 12571:2013. Specimens were oven-dried following ISO 12570:2000 until achieving constant mass (≤0.1% weight variation over 24-h intervals). Dry mass (m_{dry}) was recorded before placing specimens in desiccators with saturated salt solutions for hygroscopic equilibrium conditioning (Fig. 1(m)(n)) (Table 2).

After a 5-week equilibration period, specimens were individually removed from desiccators and weighed on an analytical balance (accuracy: ±1 mg) within 10 s to minimize moisture exchange with ambient air (Fig. 1(o)(p)). Triplicate measurements per group ensured statistical reliability, with results expressed as mean ± standard deviation. Equilibrium was defined as a mass variation of less than 0.1 wt% over a 72-h period. The final mass at each target RH was then recorded as the wet mass (m_{wet}).

2.5. Sorption isotherm model development

Equilibrium moisture content ($u_{(\varphi)}$) was calculated using

$$u_{(\varphi)=}\frac{m_{wet}(\varphi)-m_{dry}}{m_{dry}}, \quad (1)$$

where $u_{(\varphi)}$ (kg/kg) is the moisture content at equilibrium, $m_{wet(\varphi)}$ represents specimen mass at target RH, and m_{dry} is the oven-dried mass. Sorption isotherms were plotted by averaging triplicate specimens per salt spray cycle group (RH vs. $u_{(\varphi)}$).

For salt-contaminated mortar, equilibrium moisture content depends on both RH and salt deposition. A salt influence factor (η_u) was defined as

$$\eta_u=\frac{u_t}{u_c}, \quad (2)$$

where u_t and u_c denote moisture content of salt-exposed and control specimens, respectively, at identical RH. Existing sorption isotherm models (Table 3) were evaluated using control specimen data. Based on the fitting results, the optimal model was selected and subsequently modified by incorporating the η_u fitting equation to account for the influence of salt content on the equilibrium moisture content under isothermal conditions.

3. Results and discussion

3.1. Salt deposition characteristics

Full-thickness chloride analysis revealed progressive NaCl accumulation in cement mortar with increasing salt spray cycles (7–35 cycles), exhibiting a linear increase from 0.885% to 1.99% salinity (Fig. 3). This trend confirms cyclic salt spray-dry exposure facilitates gradual salt ingress, contrasting with immersion methods where equivalent salinity (0.87%–0.885%) requires concentrated NaCl solutions over shorter durations (Bai et al., 2021; He et al., 2023). The coefficient of variation (CV) across triplicates (0.51%–1.78%) remained negligible relative to absolute salinity magnitudes.

NaCl transported into cement mortar pores via capillary action resides in two distinct phases: (i) Cl^- ions electrostatically adsorbed onto pore walls, and (ii) crystalline NaCl precipitates within pore spaces (Li et al., 2023, 2024b). Specimens were dried, homogenized, and analyzed for total Cl^- content (adsorbed ions + crystalline precipitates) to quantify bulk salinity—a critical parameter linking salt deposition to pore structure modification and enhanced hygroscopicity. Phase-specific discrimination (adsorbed vs. precipitated NaCl) necessitates microstructural characterization, including X-ray diffraction (XRD) and Raman spectroscopy.

3.2. Sorption isotherm behavior

Following three months of hygroscopic equilibrium in controlled humidity chambers (33%–93% RH), cement mortar specimens exhibited distinct surface hydration behaviors (Fig. 4(a–e)). At ≤75% RH (33%, 53%, 75%), specimens maintained dry surfaces irrespective of NaCl deposition. In contrast, salt-laden specimens (Groups 3D1-1–3D3-5 and 3E1-1–3E3-5) exposed to 85% and 93% RH developed liquid films via NaCl deliquescence, while salt-free controls (Groups 3O1-4–3O3-4 and 3O1-5–3O3-5) remained dry. These findings demonstrate that NaCl deliquescence exclusively drives liquid-phase water formation above 75% RH in salt-contaminated specimens, underscoring a humidity-triggered phase transition mechanism. This confirms the critical role of environmental humidity in modulating salt-induced hygroscopicity, necessitating advanced sorption isotherm modeling to quantify such interactions.

As shown in Fig. 5(a), sorption isotherms of cement mortar specimens subjected to 7–35 salt spray cycles and control groups reveal distinct moisture uptake behaviors. Across 33%–93% RH, salt-laden specimens exhibited higher equilibrium moisture content than controls, with values increasing proportionally to cycle counts—confirming that NaCl deposition amplifies hygroscopic capacity. Figure 5(b) reveals that the moisture increase from salt spray cycles varies significantly with ambient humidity: moisture content increments were marginal at low RH (33%–55%) but escalated progressively above 75% RH, attaining the most pronounced increases within 85%–93% RH. This underscores the synergistic influence of salt deposition and ambient humidity on hygroscopicity.

Table 3 Classical fitting equations for sorption isotherms.

Equation	Formula
BET (Brunauer et al., 1938)	$u = k_1\phi/[(1+k_2\phi)(1-k_3\phi)]$
Oswin (Oswin, 1946)	$u = k_1[\phi/(1-\phi)]^{k_2}$
Caurie (Caurie, 1970)	$u = \exp(k_1+k_2\phi)$
Henderson (Henderson, 1973)	$u = \{[\ln(1-\phi)]/k_1]\}^{k_2}$
Peleg (Peleg, 1993)	$u = k_1\phi^{k2} + k_3\phi^{k4}$
GAB (Berg and Bruin, 1981)	$u = k_1k_2k_3\phi/[(1-k_1\phi)(1-k_2\phi+k_2k_3\phi)]$
Feng (Feng, 2014)	$u = \ln[(100\phi+1)^{k_1}/(1-\phi)^{k_2}] + k_3\exp(100\phi)$
Exponential	$u = k_1 + k_2e^{k_3x}$

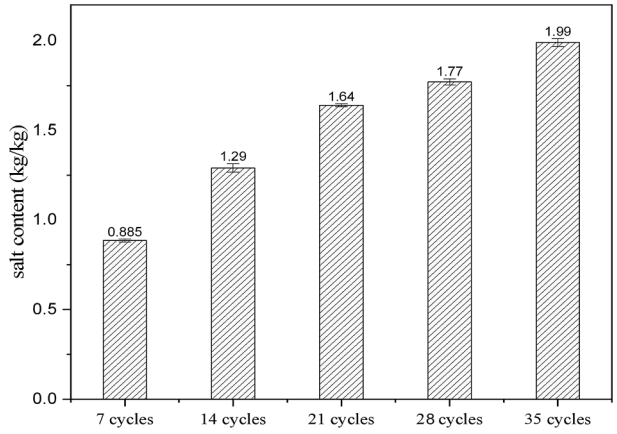

Fig. 3 Salt content of cement mortar specimens under cyclic salt spray exposure.

The isotherm slopes in Fig. 5(a) further delineate two regimes: gradual moisture uptake below 75% RH versus exponential growth above it. Salt-contaminated specimens showed significantly steeper slopes in the high-RH regime, with cycle count correlating positively to moisture amplification. This abrupt transition is attributed to the deliquescence of NaCl at its critical humidity threshold—75% RH at 20 °C (Bahadur and Russell, 2008). Below this threshold, NaCl remains crystalline, but above it, the crystals dissolve into highly hygroscopic brine, amplifying moisture uptake (Koronthalyova et al., 2015; Lubelli et al., 2004). Measurement uncertainties, attributed to material heterogeneity and salt distribution variability, exhibited standard deviations negligible relative to data magnitudes (Fig. 5(a)(b)).

Consistent with Feng's (2014) findings on aerated concrete and calcium silicate boards, control mortar specimens displayed steep moisture surges above 75% RH, indicating pronounced RH sensitivity in porous materials under high humidity. NaCl deposition exacerbates this sensitivity through deliquescence-driven phase transitions, where minor RH increases trigger disproportionate moisture uptake.

To quantify the synergistic effects of environmental humidity (ϕ, %) and salt content (C, kg/kg) on equilibrium moisture content (u_t) in salt-deposited cement mortar, two normalized factors were defined: Humidity influence factor

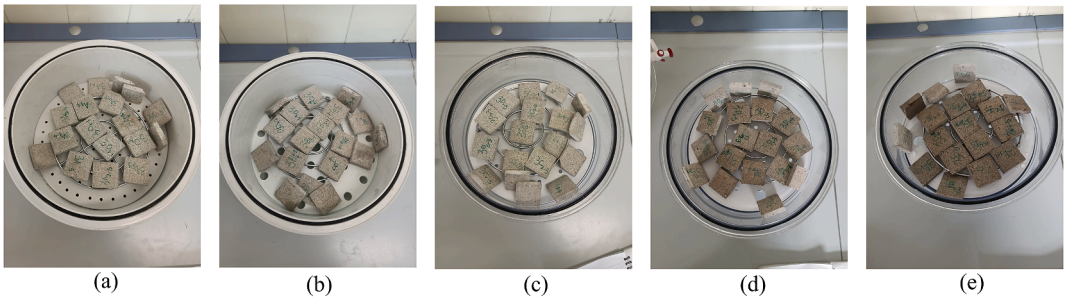

Fig. 4 Morphology of cement mortar specimens after reaching hygroscopic equilibrium at 33%—93% RH. (a) 33%; (b) 53%; (c) 75%; (d) 85%; (e) 93%.

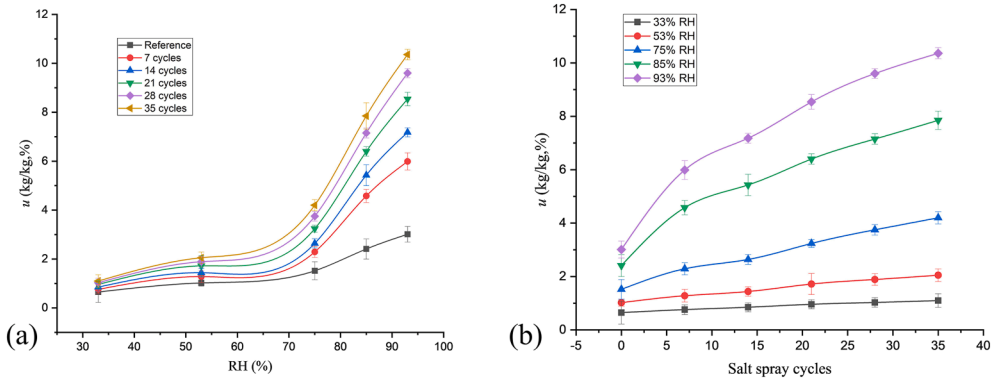

Fig. 5 Sorption isotherms of cement mortar under different humidity conditions and salt spray cycles. (a) Relative humidity dependence; (b) salt spray cycle dependence.

($\eta_{u(\phi)}$): Calculated relative to 33% RH baseline (Fig. 6(a)), and salinity influence factor ($\eta_{u(C)}$): Calculated relative to salt-free controls (Fig. 6(b)).

The $\eta_{u(\phi)}$ curves exhibited biphasic behavior: gradual growth below 75% RH and exponential escalation above this threshold (Fig. 6(a)). In contrast, the $\eta_{u(C)}$ curves shown in Fig. 6(b) displayed less pronounced, nearly linear growth ($\eta_{u(C)}$: 1.17–3.44 vs. $\eta_{u(\phi)}$: 1.84–11.57), confirming humidity as the dominant sorption driver, with salinity playing a secondary influence owing to its limited concentration range (0.885–1.99 wt%). Salt deposition significantly increases moisture content above 75% RH, resulting in elevated pore water volume and reduced air-filled porosity. This, in turn, raises thermal conductivity, impairs insulation efficiency, and exacerbates HVAC energy consumption in coastal buildings—posing critical challenges to energy efficiency and long-term sustainability in high-humidity climates.

3.3. Segmented sorption isotherm model development

As demonstrated by the sorption isotherms (Fig. 5) and influence factor fitting curves (Fig. 6), the equilibrium moisture content of cement mortar is governed by the interactive effects of environmental humidity (ϕ) and salt content (C). Accordingly, classical sorption isotherm models were modified using dual-factor fitting equations. Furthermore, based on the deliquescence mechanisms revealed by the Robinson-Stokes equation and Nielsen formula, the isothermal sorption models for salt-contaminated specimens at RH > 75% were calibrated. Finally, the three newly developed segmented fitting equations were subjected to validity verification and comparative analysis. The model development assumes that the material's pore size is significantly smaller than the model's characteristic dimension, the ambient temperature remains constant during sorption, and local temperature fluctuations caused by endothermic/exothermic processes of salt crystallization-deliquescence phase transitions are ignored.

3.3.1. Factor-modified sorption isotherm equations

A humidity-driven inflection at 75% RH (NaCl deliquescence threshold) demarcates distinct regimes in salt-mediated hygroscopic behavior. The composite influence factor (η_u)) is defined as a piecewise function of relative humidity (ϕ, %) and salt content (C, kg/kg):

$$\eta_u = \begin{cases} a_1 C \times 10^2 + a_2)(a_3\phi + a_4), \phi \le 0.75; \\ a_5 C \times 10^2 + a_6)(a_7\phi + a_8), \phi > 0.75. \end{cases} \quad (3)$$

Coefficients a_1-a_8 were determined through nonlinear least-squares regression (Levenberg-Marquardt algorithm) in Origin (2019b), minimizing the residual sum of squares (RSS) between experimental moisture content data and model predictions across all salt spray cycles (0–35 cycles) and RH conditions (33%–93%). This factor scales the optimal salt-free sorption function $f(\phi)$ to predict moisture content in saline mortar:

$$u_t = \eta_u f(\phi). \quad (4)$$

Fitting the data from salt-free specimens with eight classical models (Table 3) (Berg and Bruin, 1981; Brunauer et al., 1938; Caurie, 1970; Feng, 2014; Henderson, 1973; Oswin, 1946; Peleg, 1993) revealed six high-accuracy models ($R^2 > 0.97$), while Henderson and GAB failed to converge. Residual analysis confirmed unbiased fits (Fig. 7). BET, Peleg, and Exponential models achieved near-identical R^2 (0.98–0.99), with Peleg and Exponential showing minimal RSS (≤0.05) (Table 4).

Leveraging the parameters determined for six distinct sorption isotherm models in Table 4 (referencing Table 3), segmented fitting equations for equilibrium moisture content of salt-contaminated specimens were developed using Eqs. (3) and (4). The first regime ($\phi \le 0.75$) is described by the equations in Table 5, whereas the second regime ($\phi > 0.75$) is governed by the equations in Table 6.

For the low-humidity regime ($\phi \le 0.75$), the BET, Oswin, and Caurie equations achieved identical $R^2 = 0.974$ (Table 5). The BET equation was selected for this regime due to its minimal residual sum of squares (RSS) (Table 4). In the high-humidity regime ($\phi > 0.75$), the Peleg and BET equations yielded the highest R^2, with the Peleg equation exhibiting superior RSS performance (Tables 4 and 6). Consequently, the segmented sorption isotherm model for salt-contaminated cement mortar integrates the BET equation (low humidity) and Peleg equation (high humidity):

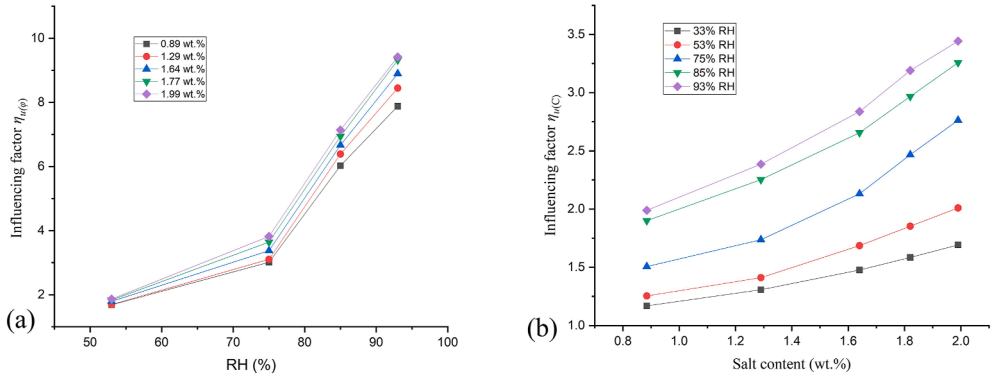

Fig. 6 Factors influencing the EMC of cement mortar: (a) humidity influence factor ($\eta_{u(\phi)}$); (b) salinity influence factor ($\eta_{u(C)}$).

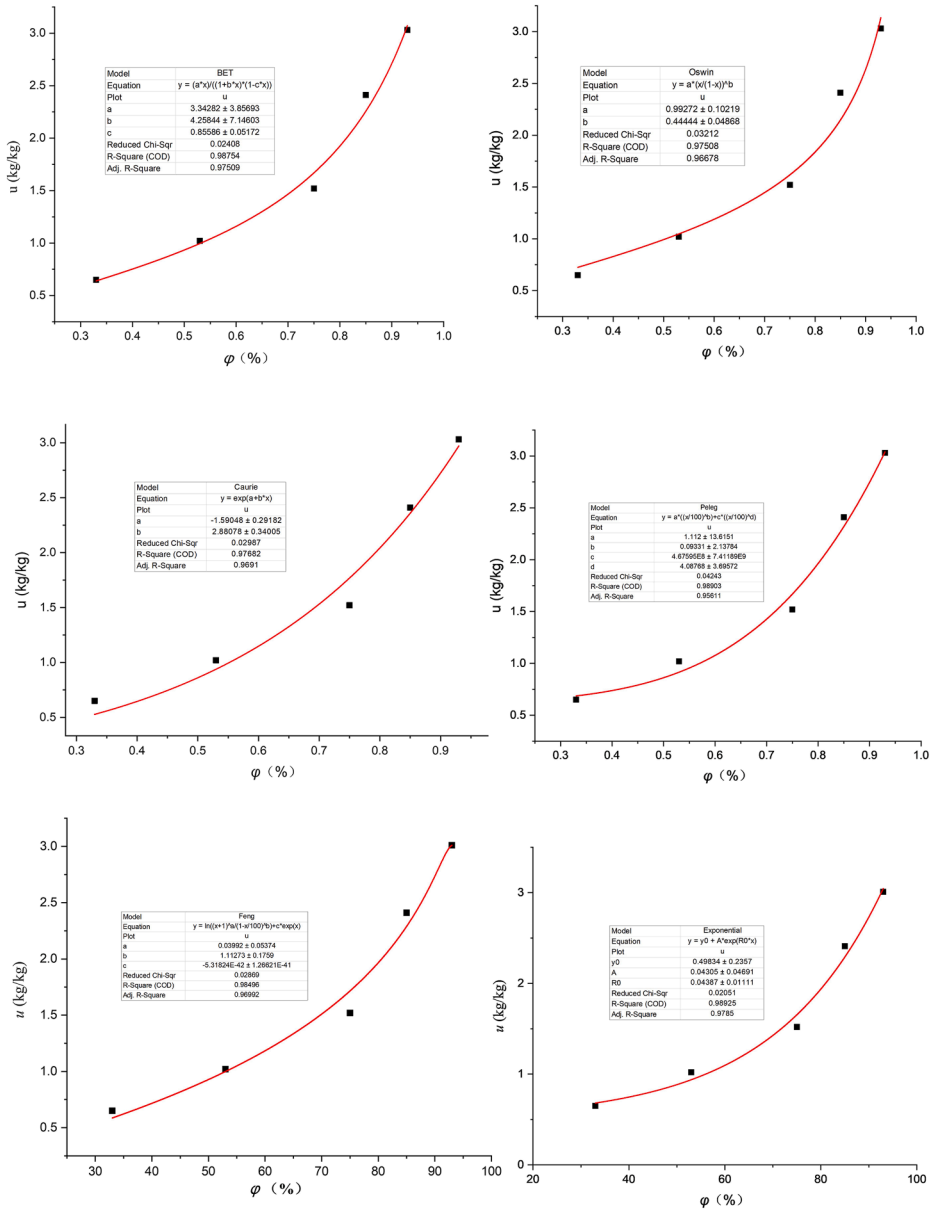

Fig. 7 Six distinct types of sorption isotherm fitting curves for cement mortar.

$$u_t = \begin{cases} \left(0.787C \times 10^2 + 92.234\right)(0.0052\phi + 0.0054)\dfrac{3.343\phi}{(1+4.258\phi)(1-0.856\phi)}, \phi \le 0.75; \\ \left(0.182C \times 10^2 + 14.965\right)(0.042\phi + 0.0048)\left(1.112\phi^{0.093} + 4.676\phi^{4.088}\right), \phi > 0.75. \end{cases} \quad (5)$$

3.3.2. High-RH fitting equations based on Robinson-Stokes theory

Salts such as NaCl undergo deliquescence when ambient humidity exceeds the water activity (a_w) of their saturated solutions. For porous materials with salt deposits, this process initiates at the critical humidity threshold (e.g., 75% RH for NaCl), where crystalline salt dissolves into a saturated solution that further dilutes with moisture absorption (Lubelli et al., 2004). The Robinson—Stokes equation governs the relationship between solution molarity (m) and humidity (ϕ) (Horvath, 1985):

$$\ln \phi = \ln a_w = -n\phi_s \cdot M_w \cdot m, \quad (6)$$

where ϕ [%] the relative humidity, a_w [%] the water activity of the salt solution, n[-] the number of ions per salt molecule, ϕ_s [-] the Osmotic coefficient of the salt solution, M_w the Molar mass of water (0.018 kg/mol), m [mol/kg] the molarity of the salt solution.

Table 4 Fitted parameters for the sorption isotherm equations of control cement mortar specimens.

Equations	k_1	k_2	k_3	k_4	R^2	RSS	Residual distribution
Oswin	0.99272	0.44444	/	/	0.975	0.09635	Random
Caurie	−1.5905	2.88078	/	/	0.977	0.08962	Random
BET	3.34282	4.25844	0.85586	/	0.988	0.04817	Random
Peleg	1.112	0.09331	4.67595	4.08768	0.989	0.04243	Random
Feng	0.0399	1.1127	−5.3182		0.985	0.05737	Random
Exponential	0.49834	0.04305	0.04387	/	0.989	0.04102	Random

Table 5 Factor-modified sorption isotherm equations for salt-contaminated cement mortar ($\phi \leq 75\%$).

Fitting equations	Equation forms	R^2
Modified BET equation	$u_t = (0.787C \times 10^2 + 92.234)(0.0052\phi + 0.0054)\dfrac{3.343\phi}{(1+4.258\phi)(1-0.856\phi)}$	0.974
Modified Oswin equation	$u_t = (0.158C \times 10^2 + 18.529)(0.04\phi + 0.0178) \times 0.993\left(\dfrac{\phi}{1-\phi}\right)^{0.444}$	0.974
Modified Caurie equation	$u_t = (0.163C \times 10^2 + 19.066)(0.002\phi + 0.0409) \times \exp(-1.59 + 2.881\phi)$	0.974
Modified Peleg equation	$u_t = (0.141C \times 10^2 + 16.465)(0.02\phi + 0.0196)(1.112\phi^{0.093} + 4.676\phi^{4.088})$	0.968
Modified Feng equation	$u_t = (0.071C \times 10^2 + 8.392)(-0.021 + 4.9228) \times \ln\dfrac{(100\phi+1)^{0.04}}{(1-\phi)^{1.113}} - 5.32\exp(100\phi)$	0.970
Modified exponential equation	$u_t = (0.213C \times 10^2 + 25.228)(0.1778\phi - 0.032)(0.498 + 0.043e^{0.0439\phi})$	0.951

Table 6 Factor—modified sorption isotherm equations for salt-contaminated cement mortar ($\phi > 75\%$).

Fitting equations	Equation forms	R^2
Modified BET equation	$u_t = (0.812C \times 10^2 + 66.838)(0.0139\phi + 0.0018)\dfrac{3.343\phi}{(1+4.258\phi)(1-0.856\phi)}$	0.981
Modified Oswin equation	$u_t = (0.203C \times 10^2 + 16.752)(0.055\phi + 0.0074) \times 0.993\left(\dfrac{\phi}{1-\phi}\right)^{0.444}$	0.974
Modified Caurie equation	$u_t = (0.205C \times 10^2 + 16.872)(0.06\phi + 0.0029) \times \exp(-1.59 + 2.881\phi)$	0.978
Modified Peleg equation	$u_t = (0.182C \times 10^2 + 14.965)(0.042\phi + 0.0048)(1.112\phi^{0.093} + 4.676\phi^{4.088})$	0.985
Modified Feng equation	$u_t = (0.131C \times 10^2 + 10.813)(-0.03\phi + 0.0087) \times \ln\dfrac{(100\phi+1)^{0.04}}{(1-\phi)^{1.113}} - 5.32\exp(100\phi)$	0.935
Modified exponential equation	$u_t = (0.317C \times 10^2 + 26.49)(0.294\phi - 0.096)(0.498 + 0.043e^{0.0439\phi})$	0.870

Salt content (C) in porous materials relates to molarity via mass balance:

$$mu_s M_N = C, \tag{7}$$

where u_s (kg/kg) the hygroscopic uptake of salt crystals per unit mass of porous material, M_N the Molar mass of NaCl (58.5 g/mol).

Combining Eqs. (6) and (7) yields the salt-derived moisture term (u_s):

$$u_s = \frac{kC}{-\ln\phi}, \tag{8}$$

where k is a calibration parameter. Assuming independent hygroscopic equilibria between the porous matrix and salt deposits, the total equilibrium moisture content (u_t) becomes

$$u_t = u_m + u_s = f(\phi) + \frac{kC}{-\ln\phi}. \tag{9}$$

Here, $u_m = f(\phi)$ represents the matrix moisture derived from salt-free isotherm models (Table 4). Using this framework, the hygroscopic uptake of NaCl crystals in cement mortar at RH > 75% was quantified. By incorporating the fitted parameters from Table 4, five superimposed sorption isotherm equations for saline cement mortar specimens were derived (Table 7). Selected by R^2, the optimal Modified BET (Table 5) and Caurie-based (Table 7) equations form segmented Eq. (10).

Table 7 Robinson-Stokes adjusted sorption isotherm equations for salt-contaminated cement mortar (RH > 75%).

Fitting equations	Equation forms	R^2
BET-based equation	$u_t = \frac{3.343\phi}{(1+4.258\phi)(1-0.856\phi)} + \frac{0.00289C \times 10^2}{-\ln\phi}$	0.944
Oswin-based equation	$u_t = 0.993\left(\frac{\phi}{1-\phi}\right)^{0.444} + \frac{0.00289C \times 10^2}{-\ln\phi}$	0.935
Caurie-based equation	$u_t = \exp(-1.59+2.881\phi) + \frac{0.00291C \times 10^2}{-\ln\phi}$	0.952
Peleg-based equation	$u_t = (1.112\phi^{0.093}+4.676\phi^{4.088}) + \frac{0.00206C \times 10^2}{-\ln\phi}$	0.933
Exponential-based equation	$u_t = (0.498+0.043e^{0.0439\phi}) + \frac{0.00419C \times 10^2}{-\ln\phi}$	0.853

$$u_t = \begin{cases} \left(0.787C \times 10^2 + 92.234\right)(0.0052\phi + 0.0054)\dfrac{3.343\phi}{(1+4.258\phi)(1-0.856\phi)}, \phi \le 0.75 \\ \exp(-1.59+2.881\phi) + \dfrac{0.00291C \times 10^2}{-\ln\phi}, \phi > 0.75 \end{cases} \quad (10)$$

3.3.3. High-RH fitting equations based on Nielsen theory

Given the hygroscopicity of salt crystals in saline porous building materials, the moisture uptake of salt crystals in air above their deliquescence relative humidity (DRH) can be calculated using the Nielsen formula (Eq. (11)).

$$u_s = \frac{c}{c_s} \times \frac{1-\phi_s}{1-\phi}, \quad (11)$$

where u_s [kg/kg] the salt-derived hygroscopic moisture content, C [%] the material salt content, C_s [kg/kg] the solubility of saturated salt solution, ϕ [%] the ambient relative humidity and ϕ_s [%] the relative humidity above the saturated salt solution. The total equilibrium moisture content (u_t) of salt-contaminated porous materials is determined by Eq. (12):

$$u_t = u_m + u_s = f(\phi) + \frac{c}{C_s} \times \frac{1-\phi_s}{1-\phi}. \quad (12)$$

For NaCl at 23 °C, C_s = 0.36 kg/kg and ϕ_s = 0.75 (Méndez-Bermúdez et al., 2016). Substituting these values and integrating parameters from Table 4, five distinct equations for u_t at RH > 75% were derived (Table 8).

According to the fitting results, the equilibrium moisture content under RH ≤ 0.75% was modeled using the BET equation from Table 5, while the Caurie model from Table 8 governed the high-humidity regime (RH > 0.75). This yielded the segmented sorption isotherm Eq. (13) for salt-deposited cement mortar.

3.3.4. Model validation and comparative performance

The fitted surfaces from Eqs. (5), (10), and (13) are shown in Fig. 8, with experimental data symmetrically distributed around these surfaces. Eq. (5) (factor-corrected method) achieved the highest coefficient of determination (R^2 = 0.98) but lacks explicit mechanistic interpretation of salt-driven sorption. In contrast, Eqs. (10) and (13) integrate deliquescence-driven moisture uptake above 75% RH through segmented superposition principles. Eq. (10) builds on the Robinson—Stokes framework, while Eq. (13) leverages the Nielsen formula, both linking solution concentration to ambient humidity to quantify salt-induced hygroscopicity.

Compared to the BET-type model employed by Bai et al. (2021), Eq. (5) adopts a segmented formulation based on distinct isotherm characteristics below and above the critical humidity threshold (75% RH), more accurately capturing moisture variation patterns in saline porous materials. While the second segment of Eq. (10) shares physical consistency with He et al.'s method (2023), its first segment calibrated via the factor-corrected approach, achieves superior accuracy (higher R^2). Notably, Eq. (13), rooted in the Nielsen framework, eliminates extraneous parameters (e.g., ion count n, osmotic coefficient ϕ_s) by directly correlating NaCl deliquescence with humidity, enhancing computational efficiency and prediction precision for salt spray-exposed materials.

$$u_t = \begin{cases} \left(0.787C \times 10^2 + 92.234\right)(0.0052\phi + 0.0054)\dfrac{3.343\phi}{(1+4.258\phi)(1-0.856\phi)}, \phi \le 0.75; \\ \exp(-1.59+2.881\phi) + \dfrac{0.00397C \times 10^2}{0.359} \times \dfrac{1-0.75}{1-\phi}, \phi > 0.75\,. \end{cases} \quad (13)$$

Table 8 Nielsen adjusted sorption isotherm equations for salt-contaminated cement mortar (RH >75%).

Fitting equations	Equation forms	R^2
BET-based equation	$u_t = \frac{3.343\phi}{(1+4.258\phi)(1-0.856\phi)} + \frac{0.00394C\times 10^2}{0.359}\times\frac{1-0.75}{1-\phi}$	0.949
Oswin-based equation	$u_t = 0.993\left(\frac{\phi}{1-\phi}\right)^{0.444} + \frac{0.00394C\times 10^2}{0.359}\times\frac{1-0.75}{1-\phi}$	0.939
Caurie-based equation	$u_t = \exp(-1.59+2.881\phi) + \frac{0.00397C\times 10^2}{0.359}\times\frac{1-0.75}{1-\phi}$	0.957
Peleg-based equation	$u_t = (1.112\phi^{0.093}+4.676\phi^{4.088}) + \frac{0.00279C\times 10^2}{0.359}\times\frac{1-0.75}{1-\phi}$	0.930
Exponential-based equation	$u_t = (0.498+0.043e^{0.0439\phi}) + \frac{0.00571C\times 10^2}{0.359}\times\frac{1-0.75}{1-\phi}$	0.866

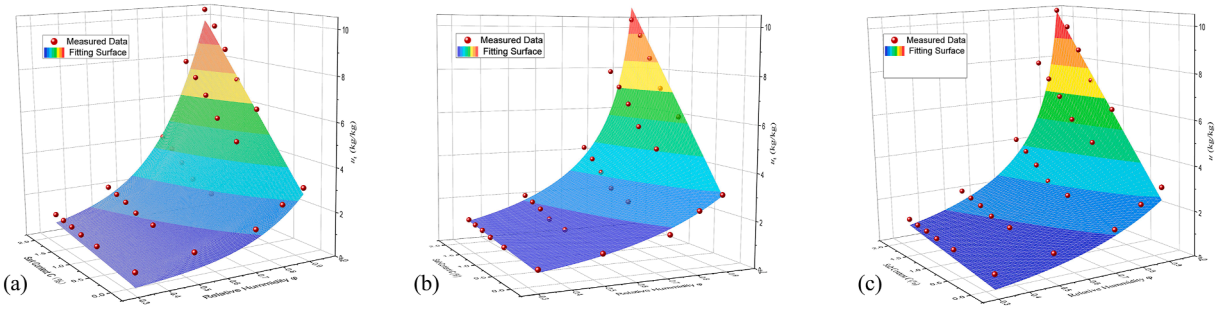

Fig. 8 Model-fitted sorption isotherm surfaces and measured data of cement mortar under salt spray conditions: (a) Eq. (5) (R^2 = 0.981); (b) Eq. (10) (R^2 = 0.952); (c) Eq. (13) (R^2 = 0. 957).

Accurate sorption isotherm determination is critical for hygrothermal load calculations in coastal buildings, where salt spray alters pore structures and hygroscopicity. Traditional equilibrium moisture measurements are time-intensive, especially for dense materials or in high-RH conditions. The proposed segmented models enable rapid moisture prediction across humidity gradients using measured salt content, thereby deriving the sorption isotherms of salt-containing building materials. Meanwhile, by modifying and importing material moisture property parameters into the editable database of the software WUFI, it is possible to accurately simulate the hygrothermal transfer performance of salt-containing building components, and further building energy consumption and thermal comfort.

3.3.5. Microstructural morphology observation

To investigate salt deposition and distribution on cement mortar under accelerated salt spray testing, optical microscopy was employed to capture surface morphology of dried specimens subjected to 7–35 salt spray cycles at specific magnifications (Fig. 9). White NaCl crystals were observed on all surfaces (front, back, and sides) of the 40 × 40 × 20 mm^3 specimens. After 7–14 cycles, sparse salt crystals preferentially adhered to the cement matrix regions (non-sand areas), forming discontinuous thin layers. With increasing cycles (21–35), salt deposits became denser (coverage >85%), filled surface pores, and evolved into continuous layers exceeding 50 μm thickness, ultimately achieving full surface coverage.

This morphological evolution microscopically reveals progressive salt accumulation on cement mortar surfaces, consistent with the chloride-ion-derived salt content trends

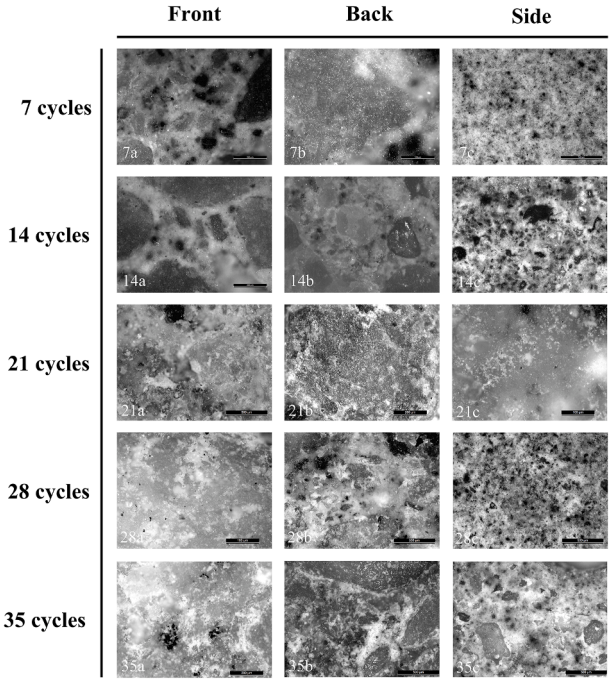

Fig. 9 Optical microscopy of cement mortar surfaces subjected to salt spray cycling.

across specimen depths (Section 3.1). Notably, NaCl crystals exhibit a deliquescence relative humidity (DRH) of 75%. Above this threshold, deposited salts deliquesce into hygroscopic brine, with higher salt content amplifying moisture adsorption capacity. These findings collectively explain the sorption isotherm trends in Fig. 5, characterized by a sudden moisture surge above 75% RH and cycle-dependent moisture enhancement (Sections 3.2). Thus, the equilibrium moisture content of saline specimens arises from the coupled effects of ambient humidity and salt crystallization/deliquescence phase transitions, as validated by both hygroscopic experiments and microstructural analyses.

4. Conclusions

To investigate the hygroscopic behavior of porous building materials in coastal salt spray climates, this study conducted accelerated salt spray exposure and isothermal sorption tests on cement mortar. By analyzing the equilibrium moisture content (u_t) across varying salt contents (C) and relative humidity (ϕ), three modified equations tailored for salt-laden cement mortar were developed. Key conclusions are as follows:

(1) Salt deposition effects: Increasing salt spray cycles elevated NaCl content (0.885—1.99 wt%), enhancing the equilibrium moisture retention of cement mortar, with isothermal sorption curves exhibiting a two-stage variation trend. Below 75% RH, all salt-contaminated specimens showed higher equilibrium moisture content than control groups, with the 35-cycle specimens demonstrating a maximum increase of 2.7%. At RH $>$ 75%, the effect of salt on enhancing equilibrium moisture content became more significant, with a 5.4%—7.4% increase observed in 35-cycle specimens. This dual-regime behavior indicates that salt-laden materials in coastal environments experience accelerated moisture accumulation above the deliquescence point, underscoring the necessity for humidity-dependent hygroscopicity models.

(2) Segmented equation development: The segmented fitting equation (Eq. (5)) was developed through a systematic two-step methodology: first, classical equations were applied to fit the isothermal sorption curves of control-group cement mortar specimens, thereby identifying the optimal baseline model. This was followed by modifying the two-stage sorption isotherms using a dual-factor fitting formula that integrates salt content (C) and ambient humidity (ϕ). Additionally, the first-segment equation (valid for RH $<$ 75%) was established via the factor-correction method. For the second segment, moisture uptake induced by salt crystal deliquescence at critical humidity—respectively described by the Robinson—Stokes equation and Nielsen formula—was incorporated. Superposition principles were then employed to derive the second-segment equations, which were subsequently integrated with the first-segment equation to formulate Eqs. (10) and (13).

(3) Equations performance: Eq. (5) achieved the highest accuracy ($R^2 = 0.981$) but was purely derived from curve characteristics, neglecting the physical mechanism of salt-induced moisture absorption. Both Eqs. (10) and (13)—based on distinct salt deliquescence theories—quantify salt-induced moisture uptake (u_s) above 75% RH, distinguishing it from inherent absorption (u_m). However, Eq. (10) relies on more parameters (e.g., ion count n, osmotic coefficient ϕ_s), increasing computational complexity and uncertainty. By contrast, Eq. (13)—Nielsen-based—correlates NaCl deliquescence with humidity, yielding $R^2 = 0.957$ (vs. Eq. (10)'s 0.952). The research innovatively integrates factor correction with a superposition theory of salt crystal deliquescence moisture uptake to quantify isothermal sorption, enabling more precise prediction of moisture content in coastal infrastructure.

Focused on sorption isotherms, the investigation excluded desorption curves to avoid inaccuracies from salt redistribution during desaturation—a process disrupting pore-scale NaCl distribution and equilibrium moisture measurements. The study specifically examined the hygroscopic behavior of cement mortar under single-salt (NaCl) deposition. Since NaCl does not chemically react with most porous building materials, changes in material hygroscopicity are primarily regulated by crystallization-deliquescence phase transitions. Consequently, these findings are applicable to other porous materials, such as aerated concrete and brick. Future research will optimize desorption experiments and assess the effects of various marine salts (e.g., $MgCl_2$, Na_2SO_4) and their mixtures in actual coastal environments.

Declaration of competing interest

The authors declare that they have no known competing financial interests or personal relationships that could have appeared to influence the work reported in this paper.

Acknowledgements

This work was financially supported by the National Natural Science Foundation of China (No. 51938006), the State Key Laboratory of Subtropical Building and Urban Science (No. 2022ZC02 and 2022KA03), the China Scholarship Council (No. 202206150001), and the Natural Science Foundation of Xinjiang Uygur Autonomous Region (No. 2025D01C12). We gratefully acknowledge the SISCON laboratory at Politecnico di Torino for access to experimental infrastructure and instrumentation. Special thanks to Prof. Elena Sesana (DIMEAS) for providing the salt spray chamber, and to Dr. Leonardo Iannucci and Prof. Sabrina Grassini (DISAT) for their technical assistance in fabricating 3D-printed specimen holders.

References

B117—2011(E) Standard Practice for Operating Salt Spray (Fog) Apparatus1.

Bahadur, R., Russell, L.M., 2008. Water uptake coefficients and deliquescence of NaCl nanoparticles at atmospheric relative humidities from molecular dynamics simulations. J. Chem. Phys. 129 (9), 094508.

Bai, L., Xie, J., Liu, J., Xie, Y., 2021. Effect of salt on hygroscopic properties of cement mortar. Constr. Build. Mater. 305, 124746.

Berg, C., Bruin, S., 1981. Water activity and its estimation in food systems: theoretical aspects. In: Rockland, L.B., Stewart, G.F. (Eds.), Water Activity: Influences on Food Quality. Academic Pressp, pp. 1—61.

Brambilla, A., Sangiorgio, A., 2021a. 5 - moisture buffering of building materials. In: Brambilla, A., Sangiorgio, A. (Eds.), Moisture and Buildings. Woodhead Publishingp, pp. 99—128.

Brambilla, A., Sangiorgio, A., 2021b. 2 - principles of hygrothermal processes. In: Brambilla, A., Sangiorgio, A. (Eds.), Moisture and Buildings. Woodhead Publishingp, pp. 9—26.

Brunauer, S., Emmett, P.H., Teller, E., 1938. Adsorption of gases in multimolecular layers. J. Am. Chem. Soc. 60 (2), 309—319.

BS EN 14147: 2003(E) Natural stone test methods. Determination of Resistance to Ageing by Salt Mist.

BS EN 197-1: 2011(E) Cement Composition, Specifications and Conformity Criteria for Common Cements.

Castellazzi, G., de Miranda, S., Grementieri, L., Molari, L., Ubertini, F., 2016. Multiphase model for hygrothermal analysis of porous media with salt crystallization and hydration. Mater. Struct. 49 (3), 1039—1063.

Caurie, M., 1970. A new model equation for predicting safe storage moisture levels for optimum stability of dehydrated foods. Int. J. Food Sci. Technol. 5 (3), 301—307.

Espinosa, R.M., Franke, L., Deckelmann, G., 2008. Phase changes of salts in porous materials: crystallization, hydration and deliquescence. Constr. Build. Mater. 22 (8), 1758—1773.

Feng, C., 2014. Study on the Test Methods for the Hygric Properties of Porous Building Materials. South China University of Technology.

Feng, C., Janssen, H., Wu, C., Feng, Y., Meng, Q., 2013. Validating various measures to accelerate the static gravimetric sorption isotherm determination. Build. Environ. 69, 64—71.

Franzen, C., Mirwald, P.W., 2009. Moisture sorption behaviour of salt mixtures in porous stone. Geochemistry 69 (1), 91—98.

He, J., Li, Q., Meng, Q., Ren, P., Li, S., Wu, H., 2023. Experimental investigation of the effect of salt on the hygroscopic properties of autoclaved aerated concrete. Constr. Build. Mater. 370, 130412.

Henderson, S.M., 1973. Equilibrium moisture content of hops. J. Agric. Eng. Res. 18 (1), 55—58.

Horvath, A.L., 1985. Handbook of Aqueous Electrolyte Solutions : Physical Properties, Estimation, and Correlation Methods.

Hung Anh, L.D., Pásztory, Z., 2021. An overview of factors influencing thermal conductivity of building insulation materials. J. Build. Eng. 44, 102604.

ISO 12570: 2000(E) Hygrothermal Performance of Building Materials and Products — Determination of Moisture Content by Drying at Elevated Temperature.

ISO 12571: 2013(E) Hygrothermal Performance of Building Materials and Products — Determination of Hygroscopic Sorption Properties.

Jamali, A., Kouhila, M., Ait Mohamed, L., Jaouhari, J.T., Idlimam, A., Abdenouri, N., 2006. Sorption isotherms of Chenopodium ambrosioides leaves at three temperatures. J. Food Eng. 72 (1), 77—84.

Khoukhi, M., 2018. The combined effect of heat and moisture transfer dependent thermal conductivity of polystyrene insulation material: impact on building energy performance. Energy Build. 169, 228—235.

Kočí, V., Vejmelková, E., Čáchová, M., Koňáková, D., Keppert, M., Maděra, J., Černý, R., 2016. Effect of moisture content on thermal properties of porous building materials. Int. J. Thermophys. 38 (2), 28.

Koniorczyk, M., Gawin, D., 2008. Heat and moisture transport in porous building materials containing salt. J. Build. Phys. 31 (4), 279—300.

Koniorczyk, M., Wojciechowski, M., 2009. Influence of salt on desorption isotherm and hygral state of cement mortar — modelling using neural networks. Constr. Build. Mater. 23 (9), 2988—2996.

Kontoleon, K.J., Giarma, C., 2016. Dynamic thermal response of building material layers in aspect of their moisture content. Appl. Energy 170, 76—91.

Koronthalyova, O., Bagel, L., Kuliffayova, M., Ifka, T., 2015. Effect of presence of salt on hygric performance of ceramic bricks. Transport Porous Media 107 (3), 667—682.

Li, B., Meng, Q., Tulliani, J.-M., Giordano, R., Li, C., Zhao, J., Ren, P., 2023. Salt migration and capillary absorption characteristics of cement mortar partially immersed in NaCl solution. J. Build. Eng. 64, 105605.

Li, B., Giordano, R., Tulliani, J.-M., Meng, Q., 2024a. Effect of sea salt on carbonation and CO2 uptake in cement mortar. Constr. Build. Mater. 438, 137212.

Li, B., Meng, Q., Giordano, R., Tulliani, J.-M., Ren, P., Wang, J., 2024b. The hygric properties of cement mortar with salt spray deposition. Constr. Build. Mater. 449, 138438.

Liu, F., Jia, B., Chen, B., Geng, W., 2017. Moisture transfer in building envelope and influence on heat transfer. Procedia Eng. 205, 3654—3661.

Lubelli, B., van Hees, R.P.J., Brocken, H.J.P., 2004. Experimental research on hygroscopic behaviour of porous specimens contaminated with salts. Constr. Build. Mater. 18 (5), 339—348.

Méndez-Bermúdez, J.G., Dominguez, H., Pusztai, L., Guba, S., Horváth, B., Szalai, I., 2016. Composition and temperature dependence of the dielectric constant of 1-propanol/water mixtures: experiment and molecular dynamics simulations. J. Mol. Liq. 219, 354—358.

Morillas, H., de Mendonca Filho, F.F., Derluyn, H., Maguregui, M., Gregoire, D., Madariaga, J.M., 2020. Decay processes in buildings close to the sea induced by marine aerosol: salt depositions inside construction materials. Sci. Total Environ. 721, 137687.

Oswin, C.R., 1946. The kinetics of package life. III. The isotherm. Journal of the Society of Chemical Industry 65 (12), 419—421.

Peleg, M., 1993. Assessment of a semi-empirical four parameter general model for sigmoid moisture sorption isotherms. J. Food Process. Eng. 16 (1), 21—37.

Peuhkuri, R.H., Rode, C., Hansen, K.K., 2005. Effect of Method, Step Size and Drying Temperature on Sorption Isotherms.

Prat, M., 2024. Evaporation, Transport, and Crystallization. Salt Crystallization in Porous Mediap, pp. 45—74.

Su, L., Niu, D., Huang, D., Luo, Y., Qiao, H., Zhang, Y., 2022. Chloride diffusion behavior and microstructure of basalt-polypropylene hybrid fiber reinforced concrete in salt spray environment. Constr. Build. Mater. 324, 126716.

Swami, S.B., Das, S.K., Maiti, B., 2005. Moisture sorption isotherms of black gram nuggets (bori) at varied temperatures. J. Food Eng. 67, 477—482.

Taher, A., Brouwers, H.J.H., 2023. Sorption isotherm measurements for porous materials: a new hygroscopic method. Constr. Build. Mater. 379, 131166.

Todorović, J., Janssen, H., 2018. The impact of salt pore clogging on the hygric properties of bricks. Constr. Build. Mater. 164, 850—863.